

A neural mass model based on single cell dynamics to model pathophysiology

Bas-Jan Zandt · Sid Visser ·
Michel J. A. M. van Putten ·
Bennie ten Haken

Received: 9 January 2014 / Revised: 24 June 2014 / Accepted: 21 July 2014 / Published online: 19 August 2014
© Springer Science+Business Media New York 2014

Abstract Neural mass models are successful in modeling brain rhythms as observed in macroscopic measurements such as the electroencephalogram (EEG). While the synaptic current is explicitly modeled in current models, the single cell electrophysiology is not taken into account. To allow for investigations of the effects of channel pathologies, channel blockers and ion concentrations on macroscopic activity, we formulate neural mass equations explicitly incorporating the single cell dynamics by using a bottom-up approach. The mean and variance of the firing rate and synaptic input distributions are modeled. The firing rate curve (F(I)-curve) is used as link between the single cell and macroscopic dynamics. We show that this model accurately reproduces the behavior of two populations of synaptically connected Hodgkin-Huxley neurons, also in non-steady state.

Keywords Mean field · Neural mass · Recurring network · Firing rate curve · Pathology · Hodgkin-Huxley · Variance · Channel blockers

1 Introduction

Neural mass models (NMM) are very successful in describing brain rhythms as measured with electroencephalogram

(EEG) (Bhattacharya et al. 2011; Victor et al. 2011; van Putten M.J. and Zandt B.J. 2013), electrocorticogram (ECoG) (Hocepiet et al. 2013), magnetoencephalogram (MEG) (Moran et al. 2013) and functional magnetic resonance imaging (fMRI) (Grefkes and Fink 2011). The main advantage of these models is that they can be mathematically analyzed due to their low dimensionality and that they are computationally inexpensive. In short, a NMM produces the average activity (firing rates) of populations of neurons. A NMM for cortex typically includes two populations, one modeling the excitatory pyramidal cells, and one the inhibitory interneurons (Wilson and Cowan 1972). If desired, NMM's can be extended with a spatial component (neural field) to model the propagation of rhythms and activations.

Neural mass models can also be used to investigate how (patho)physiological changes in the brain affect EEG rhythms. For example, they were recently used to show how the effects of anesthetics/sedatives (Hindriks and Putten 2012; Victor et al. 2011; Hutt 2013) and selective synaptic damage (Tjepkema-Cloostermans et al. 2013) result in the patterns observed in EEG's from patients under sedation and with ischemic damage, respectively.

The models contain explicit expressions for the synaptic response functions (see Fig. 1). Therefore, it is clear how to incorporate factors that alter the synaptic responses. For instance, propofol prolongs this response, which can be incorporated in a NMM by increasing the synaptic time constants (Hindriks and Putten 2012). However, an explicit relation between the sigmoidal function that converts the mean membrane potential to an output firing rate and the dynamics of single cells is missing. Therefore, it is not trivial how to correctly adapt the sigmoid to model the EEG of patients with conditions that alter the dynamics of the individual neuron, like those induced by voltage-

Action Editor: Michael Breakspear

B. -J. Zandt (✉) · M. J. A. M. van Putten · B. ten Haken
MIRA - Institute for Biomedical Technology and
Technical Medicine, University of Twente, P.O. Box 217,
7500, AE Enschede, The Netherlands
e-mail: b.zandt@utwente.nl

S. Visser
School of Mathematical Sciences, University of Nottingham,
University Park, NG7 2RD, Nottingham, UK

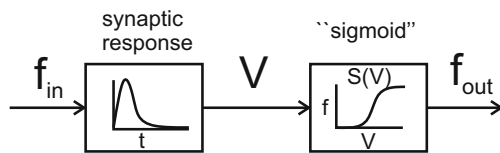


Fig. 1 Diagram of a neural mass model describing one population with one input. The input to a population f_{in} , i.e. the presynaptic firing rate, drives the dynamics of the state of the population, represented by the population potential V . The response of V to f_{in} represents the dynamics of the synapses and the membrane potential of the dendrites and soma. This state is subsequently converted into the output firing rate f_{out} by a sigmoidal function $S(V)$

gated channel blockers, channel mutations or changes in ion concentrations. Such factors play an important role in the (patho)physiology of patients with ischemia, traumatic brain injury, epilepsy and migraine (Dreier 2011; Bazhenov et al. 2008; Meisler and Kearney 2005; Somjen 2001).

In this paper we aim to provide a straight-forward bottom-up description that relates a NMM to the dynamics of the single cells and their connectivity. From this description, we construct a new neural mass model. In particular, we investigate the relation of the sigmoid to the single cell dynamics and their connectivity, by describing the dynamics of a network of excitatory and inhibitory conductance based cells (see Fig. 2). We confirm that our newly proposed neural mass model accurately reproduces the dynamics observed in a network of spiking neurons.

To take the influence of the connectivity in the network into account, we study the distributions of firing rates and input currents of the neurons. The dynamic evolution of these distributions is then expressed up to second order, i.e. mean and variance. The distribution of input currents yields, together with the F(I)-curves, the distribution of firing rates within the population. Changes in electrophysiological parameters of the cells typically shift and/or stretch

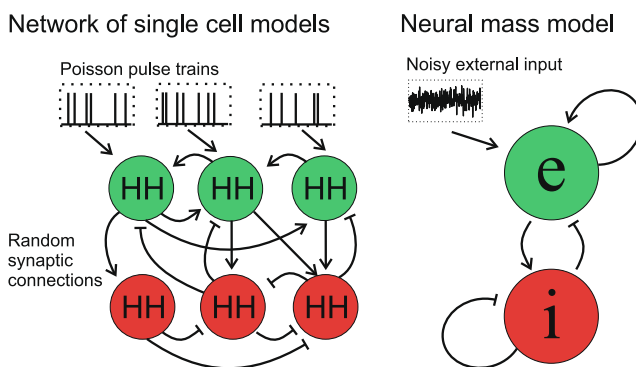


Fig. 2 The approach we use for modeling neural dynamics. A network of spiking neurons is taken as starting point (left). It consists of two populations of synaptically coupled Hodgkin-Huxley (HH) neurons. The new model we will construct, a neural mass model (right), describes the average dynamics of each population

these F(I)-curves. The well-known Hodgkin-Huxley (HH) model is used as single cell model because it is the simplest model which is fully expressed in physiological parameters. Our approach is general, though, and allows for relating a neural mass model to networks of other single cell spiking models as well.

First, we discuss the interpretation of the variables which commonly appear in a neural mass model and some critical issues with the classical derivation of the sigmoidal function. Then we describe our NMM that includes the single cell dynamics, its implementation in Matlab, and validate this new model with a network of spiking cells.

1.1 Neural mass modeling

We discuss the typical parameters and variables of a neural mass model, and their interpretation. The model from (Liley et al. 2002) is used as example.

The variable representing the state of a population is the population potential V (denoted h in (Liley et al. 2002)). The EEG signal is assumed to be proportional to V . It is interpreted as the average membrane potential of the cells' somas. V is obtained by low-pass filtering the input spike rate to the population with a set of differential equations. Their impulse response is the postsynaptic potential (PSP) of a neuron, i.e. the response of the post-synaptic conductance and subsequently the post-synaptic membrane voltage to a presynaptic spike:

$$I_{syn,x} = H * f_x \quad (1)$$

$$\tau \frac{dV}{dt} = V_{rest} - V + \sum_x \psi I_{syn,x}, \quad (2)$$

where x denotes the populations from which input is received (i.e. excitatory and inhibitory population), $H * f_x$ is the synaptic impulse response convoluted with the presynaptic firing rate, τ is the membrane time constant, V_{rest} is the resting potential and ψ is the synaptic effectiveness. This effectiveness depends weakly on V . $I_{syn,x}$, with $x = e, i$, are the synaptic activations of the synapses originating from the two populations. Liley et al. chose alpha synapses in their model, for which the convolution with H corresponds to a second order differential equation.

Subsequently, V is converted to an output firing rate of the population through a sigmoidal function $S(V)$. A symmetric sigmoid is derived under the assumption that a cell is either active (firing) or not, and a cell is assumed active when its membrane potential is above its spiking threshold. Furthermore it is assumed that either all cells receive the same input, but have different voltage thresholds, or the variation in spiking threshold is relatively small, while the variation in input or noise causes cells to have different

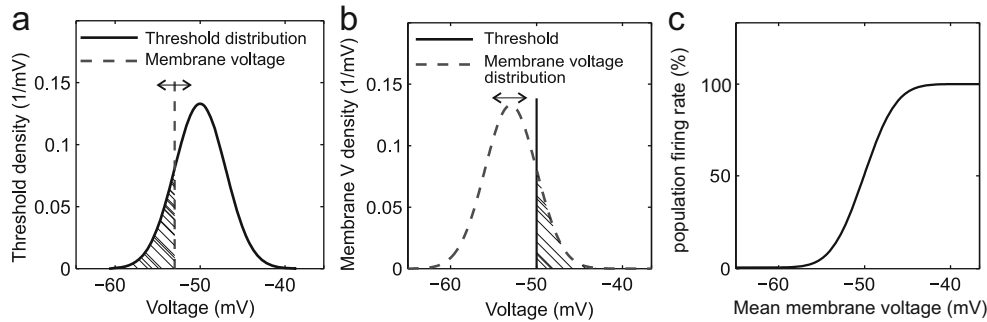


Fig. 3 Visualization of calculating the sigmoidal voltage-to-spike-rate function (c), from either an assumed Gaussian distribution of the spiking thresholds (a) or the induced membrane voltages of the neurons (b). The hatched area is the part of the population that has a membrane

voltage above threshold and is considered to be spiking. The double headed arrow denotes that the average membrane voltage can vary in time

membrane potentials. These two interpretations are visualized in Fig. 3. When Gaussian distributions are assumed, either assumption results in a sigmoid that is the integral of a Gaussian curve (Wilson and Cowan 1972). For simplicity, the sigmoid resulting from this integral is often replaced by a similarly shaped function, as done by (Wilson and Cowan 1972):

$$\begin{aligned}
 S(V) &= f_{\max} \int_{-\infty}^V \frac{1}{\sigma\sqrt{2\pi}} \exp\left\{-\frac{(V'-\mu)^2}{2\sigma^2}\right\} dV' \\
 &= f_{\max} \left(\frac{1}{2} + \frac{1}{2} \operatorname{erf}\left(\frac{V-\mu}{\sqrt{2}\sigma}\right)\right) \\
 &\approx \frac{f_{\max}}{1 + \exp(\sqrt{2}(\mu-V)/\sigma)},
 \end{aligned}
 \tag{3}$$

where μ is the threshold voltage, σ is the width of the voltage distribution and f_{\max} is the firing rate of a single neuron when active, i.e. the maximum mean firing rate of the population.

These derivations assume a constant firing rate of the cells when above threshold (so-called McCulloch-Pitts neurons), contrary to the fact that neurons have an increasing firing rate for increasing input currents. Furthermore, a constant width of the dispersion of the states of the neurons is assumed, although this width may depend greatly on the synaptic input (Marreiros et al. 2008). Still, the models using this sigmoid are successful, because they are operated on only a small part of the $f = S(V)$ curve, with parameters that are fitted to reproduce experimental data. Therefore, an exact determination of the entire sigmoidal firing rate curve from a physiological basis is often not necessary to obtain realistic results. This means that the sigmoidal curve is de facto phenomenological, despite the fact that its parameters suggest to be physiological.

Another issue is that the interpretation of “the membrane voltage of a cell” is not clear in the derivations above, especially not for spiking cells. Two interpretations are (Holt 1997): 1, the hypothetical membrane potential of the somas, if they had been passive (linear). The somas with a potential above threshold are actually spiking. 2, the postsynaptic membrane voltage of the dendritic cable. In this case, the

dendritic membrane voltage induces an input current into the soma that, when large enough, generates action potentials. It can be shown that the reaction time of the population is too slow when using the first interpretation of passive somas (Holt 1997). Therefore we will adhere to the second interpretation. This means that $V - V_{\text{rest}}$ is interpreted as a measure for the input current a cell receives, following Ohm’s law.

For a more in-depth discussion of the derivation of neural mass models, we recommend the excellent review from Deco et al. (Deco et al. 2008).

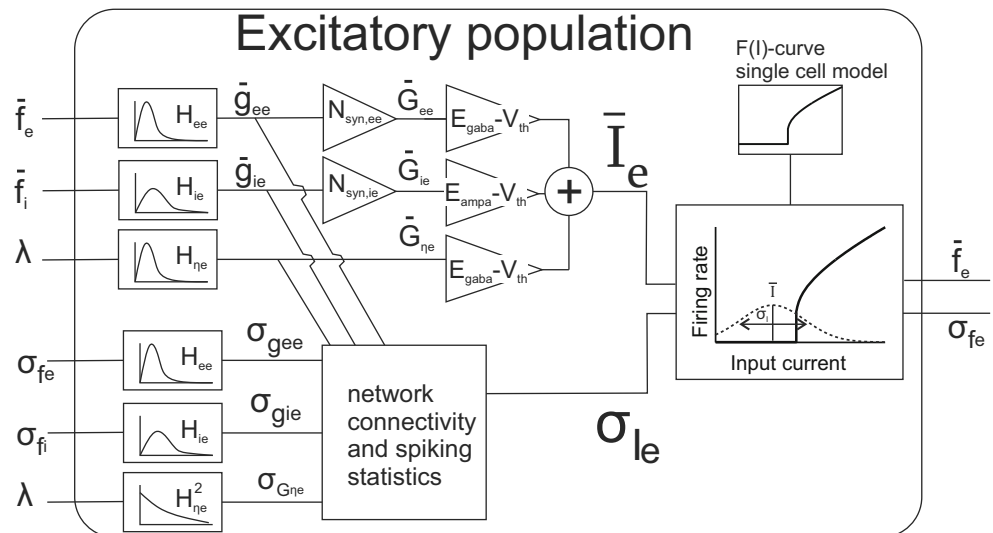
2 Constructing a new neural mass model

We aim to construct a neural mass model as depicted in Fig. 2, with an excitatory and an inhibitory population, synaptically connected to themselves and each other with the excitatory population receiving external input. In this section, we will derive the average behavior of a population of neurons from the properties of a network of synaptically connected cells, by describing the statistics of the synaptic inputs and the firing rates.

The sigmoidal function describing the response of the population will be derived by smoothing the F(I)-curve of the single cells with the distribution of the input current over the cells. Therefore, we will calculate not only the mean input and output, but also their variances. Note that throughout this work the terms mean and variance denote the instantaneous distribution over the cells in a population, i.e. the ensemble, not a distribution over time.

Figure 4 shows schematically our macroscopic model for the excitatory population and the synapses that project onto these cells. The schematic for the inhibitory population is similar, but without external input $\lambda(t)$. The excitatory population (e) receives excitatory input from itself and from an external source (η), and inhibitory input from the inhibitory population (i). The mean $\bar{f}(t)$ and variance $\sigma_f(t)$ of the fir-

Fig. 4 Schematic of the excitatory population in the neural mass model. The population receives input from the excitatory and inhibitory populations, as well as excitatory external input λ , with firing rates with mean \bar{f} and variance σ_f . These are convoluted with their synaptic responses to yield the conductances of the single synapses (mean \bar{g} and variance σ_g). These are the state variables in the model. From these the input currents are calculated (mean \bar{I} and variance σ_I). Together with the single cell F(I)-curve, they produce the output firing rates



ing rates of the three input sources are convoluted with the corresponding impulse response H . This yields the mean $\bar{g}(t)$ and variance $\sigma_g(t)$ of the corresponding synaptic conductances. These are the dynamical state variables in our model. These in turn are combined into the mean $\bar{I}(t)$ and variance $\sigma_I(t)$ of the input currents into the cells, from which the mean and variance of the output firing rates are calculated. We will derive the model step by step, starting with the output.

In deriving our model, we make several assumptions on the general behavior and connectivity of the neurons. First, as common for neural mass models (Deco et al. 2008), we assume that exact spike timings are not important for the network dynamics and there is no synchronization of spike timings within the population. Therefore, the activity of neurons is described as their firing rate.

Furthermore, we consider the inhomogeneity of the output of the cells within a population, i.e. of their firing rates. We assume the main contribution to this inhomogeneity comes from the differences in synaptic inputs the cells receive (Manwani and Koch 1999), with a small additional contribution from the inhomogeneities in the single cell properties. We do not take the effects of noise from e.g. stochastic opening of ion channels into account. The synaptic connectivity is considered to be inhomogeneous, rather than all-to-all. For the sake of discussing our model, the neurons are assumed to be sparsely connected, although this is not strictly necessary. The connectivity is assumed to be essentially unstructured, such that for each postsynaptic neuron the set of presynaptic firing rates can be considered to be independently drawn subsets of the firing rates of all presynaptic neurons. From these assumptions it follows that there are no distinguishable subsets of neurons within a population and the total synaptic inputs of the individual neurons are more or less synchronous.

Finally, the number of postsynaptic neurons in a population is assumed to be large enough to describe the input currents and resulting firing rates as a continuous distribution.

2.1 The firing rate of a population: the sigmoid function

In this section we derive a sigmoidal function from the distribution of input currents over the cells. We assume these to be normally distributed and neglect higher order moments of the distribution:

$$I(t) \sim N(\bar{I}(t), \sigma_I^2(t)). \quad (4)$$

Hence, the mean $\bar{I}(t)$ and variance $\sigma_I^2(t)$ fully characterize the distribution function $\phi(I; t)$ as:

$$\begin{aligned} \phi_y(I; t) &:= \phi(I; \bar{I}_y(t), \sigma_{I_y}(t)) \\ &= \frac{1}{\sigma_{I_y}(t)\sqrt{2\pi}} \exp\left(-\frac{1}{2}\left(\frac{I - \bar{I}_y(t)}{\sigma_{I_y}(t)}\right)^2\right). \end{aligned} \quad (5)$$

Throughout this paper, the subscript x denotes the presynaptic population or source (e,i, η) and y the postsynaptic population (e,i).

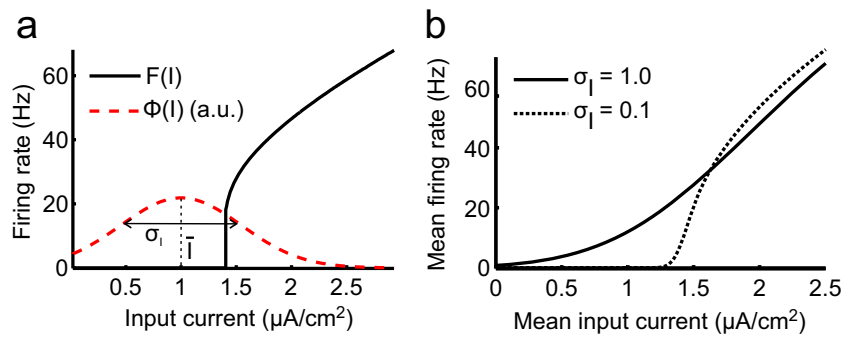
The mean $\bar{f}_y(t)$ and variance $\sigma_{f_y}^2(t)$ of the output firing rates can be calculated from the input current distribution and the F(I)-curve, as depicted in Fig. 5a:

$$\bar{f}_y(t) = \int F_y(I) \phi(I; \bar{I}_y(t), \sigma_{I_y}(t)) dI \quad (6)$$

$$\sigma_{f_y}^2(t) = \int (F_y(I) - \bar{f}_y(t))^2 \phi(I; \bar{I}_y(t), \sigma_{I_y}(t)) dI. \quad (7)$$

In order for this to be valid, the F(I)-curve must yield a good approximation for the instantaneous firing rate of neurons receiving fluctuating input currents. This is the case when these fluctuations are on a time scale, as determined by the synaptic integration time, that is much slower than the

Fig. 5 The functions involved in calculating the firing rate distribution. **(a)** The distribution of the input currents and the F(I)-curve and **(b)** the resulting sigmoidal function, depending on σ_I



interspike interval. We will empirically show in the Results that this assumption can be relaxed to the time scales being similar. Furthermore, the F(I)-curve must be well-defined, which assumes the neurons show simple behavior, i.e. do not show resonances, bistability or bursting. Note that the firing rates are not required to be normally distributed.

To obtain a sigmoid function in familiar form, Equation (6) is equivalently described as the F(I)-curve smoothed by convolution with a Gaussian of width $\sigma_I(t)$:

$$\bar{f}_y(t) = S_y(\bar{I}_y(t); \sigma_{I_y}^2(t)). \tag{8}$$

The resulting sigmoid function S now depends on $\sigma_I(t)$, as shown in Fig. 5b.

We have now derived a sigmoid function based on the firing rate curve of the cells in the population, as was our main aim. The F(I)-curve can be calculated numerically or analytically from the single cell model. The output firing rate distribution ($\bar{f}_y(t)$ and $\sigma_{f_y}^2$) is a function of $\bar{I}(t)$ and $\sigma_I(t)$. These will be calculated from the input firing rates in the next sections.

2.2 Distribution of the synaptic conductance

Presynaptic activity causes the synapses to release neurotransmitter. This in turn opens ion channels on the postsynaptic membrane, increasing the conductance of these channels, which generates a synaptic current. The distribution of the input current will be calculated from the synaptic conductances.

We assume that cells in the network are randomly connected with synapses. These connections possibly have different strengths (weights). Cells receive synaptic connections from different populations and we refer to the group of all synapses from source x to population y as the synaptic population xy . Our model contains five synaptic populations, specifically ee, ie, ηe , ei, and ii (see Figs. 2 and 4). The conductances of the single synapses and their summation by the postsynaptic neurons are calculated in Appendix A. The derived expressions used in the neural mass model are summarized in this section.

The mean and variance of the conductance of the individual synapses g_{xy} are obtained from the presynaptic firing rates f_x (Appendix A), by assuming a linear synaptic response:

$$\bar{g}_{xy} = H_{xy} * \bar{f}_x(t) \tag{9}$$

$$\sigma_{g_{xy}} = H_{xy} * \sigma_{f_x}(t). \tag{10}$$

H is the synaptic impulse response, i.e. PSP, of a single synapse and the asterisk denotes a convolution.

Although the form of Equation (10) is simple, the derivation is not trivial. In its derivation the presynaptic cells are assumed to fire periodically. In contrast, for the external input we assume Poisson (shot noise) statistics. Assuming all postsynaptic cells receive external input at the same rate λ , the mean and variance of the externally induced synaptic conductance are calculated as (Amit and Brunel 1997):

$$\bar{G}_\eta = H_{\eta e} * \lambda \tag{11}$$

$$\sigma_{G_\eta}^2 = H_{\eta e}^2 * \lambda. \tag{12}$$

For each single neuron in population y , we define the total conductance G_{xy} as the sum of the contributions of the individual synapses from source x . The distribution of G_{xy} is determined (Appendix A) from the connection matrix. The mean \bar{G}_{xy} is expressed as:

$$\bar{G}_{xy}(t) = \bar{N}_{\text{syn},xy} H_{xy} * \bar{f}_x(t), \tag{13}$$

where N_{syn} is the mean (weighted) number of synaptic connections a neuron receives.

The variance $\sigma_G(t)$ is expressed as (Appendix A):

$$\sigma_{G_{xy}}^2(t) = \text{var}(N_{\text{syn},xy}) \bar{g}_{xy}(t)^2 + N'_{\text{syn},xy} \sigma_{g_{xy}}^2(t). \tag{14}$$

The first term is the variance due to differences in the number of synaptic connections received by the cells, the second term is the variance due to the variance in firing rates of the presynaptic neurons. N'_{syn} is the expected (weighted) number of connections a postsynaptic neuron does not share with a random other cell of its population. This number is zero for an all-to-all connected network and approximately equal to N_{syn} for a very sparsely connected network.

2.3 Distribution of the input current

With the expressions for the total synaptic conductances the distribution of the input current can be calculated. The total input current I_e into a single cell in the excitatory population is calculated from the conductance of the three sources of input (see Fig. 4) as:

$$I_e(t) = (E_{\text{ampa}} - V_{\text{th}}) G_{ee}(t) + (E_{\text{gaba}} - V_{\text{th}}) G_{ie}(t) + (E_{\text{ampa}} - V_{\text{th}}) G_{\eta e}(t) + \Delta I. \quad (15)$$

The expressions for the inhibitory population are similar. ΔI is an effective synaptic input, added to simulate heterogeneity of the single cell parameters. $E_{\text{ampa/gaba}}$ is the reversal potential of the excitatory/inhibitory synapses, G_{xy} the total synaptic conductance induced by population x on a neuron in population y and η the conductance induced by external input. V_{th} is the threshold potential of the neuron. Usually, the membrane voltage itself, rather than the threshold voltage, is used to calculate the input current. However, V_{th} yields a good approximation to determine the spike rate, as detailed in Appendix B. This approximation neglects the shunting effect of the synaptic conductances. Subthreshold input currents are calculated incorrectly, but this is inconsequential, since the spike rate will be determined correctly as zero.

Assuming the distribution of the total conductances from the different sources are independent, the mean and variance of the input current are calculated as:

$$\bar{I}_e(t) = (E_{\text{ampa}} - V_{\text{th}}) \bar{G}_{ee}(t) + (E_{\text{gaba}} - V_{\text{th}}) \bar{G}_{ie}(t) + (E_{\text{ampa}} - V_{\text{th}}) \bar{G}_{\eta e}(t), \quad (16)$$

$$\sigma_{I_e}^2(t) = (E_{\text{ampa}} - V_{\text{th}})^2 \sigma_{G_{ee}}^2(t) + (E_{\text{gaba}} - V_{\text{th}})^2 \sigma_{G_{ie}}^2(t) + (E_{\text{ampa}} - V_{\text{th}})^2 \sigma_{G_{\eta e}}^2(t) + \sigma_{\Delta I}^2. \quad (17)$$

These expressions close our set of equations, which can now in principle be analyzed and simulated. First however, more computationally efficient expressions for the convolutions Eqs. (10–12) will be given in the next section.

2.4 Differential equations for the synaptic dynamics

For computational efficiency as well as analytical tractability, a synaptic impulse response H is chosen such that the convolutions can be described with ordinary differential equations. Common choices are the exponential and the alpha synapse (De Schutter 2010), with impulse responses (PSP's) of

$$H_{\text{exp}} = g_0 e^{-t/\tau} \quad (18)$$

and

$$H_{\alpha} = e g_0 \frac{t}{\tau} e^{-t/\tau}, \quad (19)$$

respectively. Here g_0 is the peak amplitude of the PSP and τ the synaptic time constant. The corresponding differential equations are:

$$\frac{dg}{dt} = -\frac{g}{\tau} + g_0 f(t) \quad (20)$$

and

$$\frac{d^2g}{dt^2} = -\frac{2}{\tau} \frac{dg}{dt} - \frac{g}{\tau^2} + \frac{e}{\tau} g_0 f(t). \quad (21)$$

The convolution with H^2 (Eq. (12)) can be written as:

$$\frac{d\sigma^2}{dt} + 2\frac{\sigma^2}{\tau} = g_0^2 f(t) \quad (22)$$

and

$$\frac{d^3\sigma^2}{dt^3} + \frac{6}{\tau} \frac{d^2\sigma^2}{dt^2} + \frac{12}{\tau^2} \frac{d\sigma^2}{dt} + \frac{8}{\tau} \sigma^2 = 2 \frac{e^2 g_0^2}{\tau^2} \lambda(t), \quad (23)$$

for the exponential and alpha synapse respectively.

We used the alpha synapses in our implementation. However, to reduce the dimensionality and improve computational efficiency when calculating the variances, H and H^2 were approximated with exponential functions. To obtain equal steady state values and approximately equal rise times, we chose approximations that have equal areas, and equal second moments around $t = 0$. This gives values of $g_0 = e/2 g_{0,\alpha}$ and $\tau = 2 \tau_{\alpha}$ for H and $g_0 = e/\sqrt{(6)} g_{\alpha}$ and $\tau = 3 \tau_{\alpha}$ for H^2 .

3 Implementation and simulations

First, we describe the implementation of a network of spiking neurons, used as a standard for validation, and then the implementation of our neural mass model.¹

3.1 Network of spiking neurons

The Norns - Neural Network Studio was used to build and simulate the network of spiking cells. Norns is designed for easy analysis of networks of spiking neuron models²

The single cells were modeled with a Hodgkin-Huxley (HH) model with voltage gated Na^+ - and K^+ -channels and leak currents (Eqs. 1–3 of (Zandt et al. 2011)). The cells were synaptically connected with alpha synapses. These were chosen since they are a second order system, which has been shown to generate more realistic frequency spectra than exponential synapses (Liley et al. 2002). Differential equations for the HH model and the alpha synapse Equation (21) were added as new cell and synapse types to

¹The simulation code is available from modelDB (Hines et al. 2004), accession nr. 155130 and Researchgate www.researchgate.net/profile/Bas-Jan_Zandt

²Available from ModelDB, accession nr. 154739.

the Norns package. An action potential (spike) was defined as the membrane voltage crossing 0 mV from below.

A network was built consisting of two populations of 100 cells each (see Fig. 2). For simplicity, the same parameters were chosen for all cells. Then, heterogeneity of the population was obtained with an additional sodium leak conductance, normally distributed over the cells. This conveniently allows us to model this heterogeneity as an extra synaptic input.

Synaptic currents were included next to the leak and voltage gated currents. They are expressed as usual as $I = g_{\text{syn}}(E_{\text{syn}} - V)$, where V is the neuron’s membrane voltage. Synaptic connections, represented in connection matrices W_{xy} , were randomly made between the cells with a probability p , all having equal strength ($w = 1$). Different strengths of the synaptic populations ($e \rightarrow e$, $e \rightarrow i$, etc.) were obtained by choosing different PSP amplitudes g_0 .

The excitatory cells were given external input via excitatory synapses, that received Poisson distributed spikes with rate λ . To show how the populations react to a change in input, a double step in input was given:

$$\lambda = \begin{cases} 0 \text{ s}^{-1} & t < 0 \text{ s} \\ 600 \text{ s}^{-1} & 0 \text{ s} \leq t < 0.5 \text{ s} \\ 400 \text{ s}^{-1} & 0.5 \text{ s} \leq t \end{cases} \quad (24)$$

The synaptic currents that are induced by this input are depicted in Fig. 6.

3.2 The new neural mass model

First, the F(I)-curve was calculated by simulating a single HH cell, as described in the previous section, for a range of constant conductivities of the excitatory synapses in the simulation. F was determined from the interspike interval (ISI). The reported I is calculated as $I = g(E_{\text{ampa}} - V_{\text{th}})$. Alternatively, a current could have been injected directly into the

cells. The former method leads to more accurate results, since it takes the shunting effect of the excitatory synaptic conductance into account. For simplicity, the neurons in the two populations were given the same parameter values and hence have the same F(I)-curve. The threshold voltage of the HH model was determined numerically, typically -55 mV. To be able to show the effects of gradually increasing the extracellular potassium concentration, multiple F(I)-curves were calculated for different potassium concentrations, with a resolution of 1 mM. These curves were linearly interpolated during the simulation. For simplicity, we assumed the threshold voltage to remain constant, since this was found not to change significantly.

The values for the parameters representing the number of synapses were calculated from the generated connection matrices W_{xy} used in the network model. For a binomial distribution with $p = 0.5$ and $N = 100$, this yields on average $\bar{N}_{\text{syn}} = 50$, $\text{var}(N_{\text{syn}}) = 25$ and $N' = 25$ for all synaptic populations, i.e. the cells receive $50 \pm \sqrt{25}$ synapses of each type, and two cells share on average 50-25 synaptic connections of each type. Note that $\text{var}(N) = N'_{\text{syn}}$ is a property of the binomial distribution.

The differential equations of the neural mass model (see method section) were implemented in Matlab. The differential equations were solved with a forward Euler time stepping algorithm, using a time step of 0.1 ms. The second order differential equation for the alpha synapse was used to calculate \bar{g} for each of the five synaptic populations. To reduce the dimensionality, σ_g was calculated using an exponential approximation (see Section 2.4). Because the variance of g has only a secondary effect on the dynamics, the errors on the firing rates and synaptic conductances introduced by this approximation are small.

A noisy input signal for the NMM was generated by binning the random external input spike times of the simulation of the network model ($\Delta t = 1 \text{ ms}$), allowing to compare the two models with the same input.

3.3 Parameters

To validate the new neural mass model, we simulated three different networks. Our standard parameter set defines a network of type 1 spiking neurons in which there is relatively weak feedback between the populations. We further tested our approach by increasing the feedback, i.e. the strength of the $i \rightarrow e$ synapses, and by simulating a network with type 2 spiking cells. This choice allows us to assess and discuss the performance of our model for both fluctuations around a steady state and limit cycle behavior, as well discuss the necessity of taking the variance of the firing rate into account. Furthermore, to demonstrate that changes in single cell dynamics can easily be incorporated, a steadily increasing extracellular potassium concentration is modeled. Such

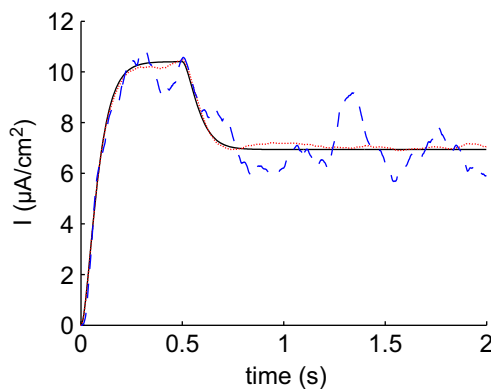


Fig. 6 Synaptic currents induced by (Poisson distributed) external input in our simulation. Depicted are the expected current (solid black line), and a typical realization for a single synapse (dashed blue line) and the mean of 100 synapses (dotted red line)

an increased concentration typically occurs in epilepsy and spreading depression.

In summary, four cases are modeled:

1. a network of type 1 spiking neurons
2. the same network with strong feedback between the populations ($g_{0\eta e} = 5.4$ and $g_{0ie} = 8 \mu\text{S}/\text{cm}^2$)
3. a network of type 2 spiking neurons
4. a network of type 1 cells with variable E_k

For the single HH cells, conductances and time constants were chosen as in (Zandt et al. 2011). Nernst potentials were chosen in the physiological range as $E_k = -95$ mV, $E_{\text{na}} = 53$ mV, $E_{\text{cl}} = -82$ mV. A type 1 neuron was created from the standard HH parameters by increasing the membrane capacitance C_m to $10 \mu\text{F}/\text{cm}^2$, while the original value of $C_m = 1.0 \mu\text{F}/\text{cm}^2$ was used to model type 2 spiking behavior. Heterogeneity of the cells was modeled by an extra sodium conductance that was normally distributed, with a width corresponding to an input current of $\sigma_{\Delta I} = 0.5 \mu\text{A}/\text{cm}^2$, approximately a third of the threshold current. Time constants were chosen based on the membrane time constants obtained in (Liley et al. 2002). These were halved, since the alpha function is wider than an exponential function, in order to obtain similar synaptic integration times. Table 1 shows the synaptic parameters. Values for the synaptic strengths were chosen such that the steady state firing rates of both populations were approximately equal in the range between 4 and 100 Hz. A mean firing rate was obtained around approximately 30 Hz by tuning the strength of the external input. The synaptic strengths of the fourth network were chosen empirically to show limit cycle behavior upon varying the potassium concentration.

4 Data analysis of the network simulations

Spike times and synaptic conductances for each cell were recorded from the network model. From the synaptic conductances, synaptic currents were calculated from the terms in Equations (16) and (17). For some simulations the fre-

quency spectrum of the synaptic current was obtained with the fast Fourier transform (FFT) of an 8 second long segment with constant input rate. The mean firing rate in the network model was determined for both populations by binning the spikes in intervals of 5 ms. The standard deviation of the firing rates were calculated from the instantaneous frequencies of the individual cells, determined by their interspike intervals. This simple method yields artifacts when the population spike rate changes rapidly. Sections with artifacts were bleached in the figures.

One of the main assumptions in the derivation of our NMM was that the firing rate of the cells in the network is determined by their instantaneous input current. To test whether this approximation was accurate, for each cell in the network the spike rate was calculated both from the recorded interspike intervals as well as from the recorded synaptic conductances, according to Equation (16).

Besides the spike timings of the external input, none of the recorded quantities were given as input to the NMM.

5 Results

We will now first validate our NMM by comparing it with simulations of a spiking network and check whether the firing rates of the single cells in the network indeed instantaneously depend on their synaptic input, as assumed in the derivation of the NMM. We then show how our neural mass model can be used to model changes in electrophysiological single cell parameters with an example of a network where the extracellular potassium concentration is gradually increased, as may occur in some pathological conditions.

5.1 Validation

Figure 7 compares the responses of our NMM with those of the spiking network model. The upper panels compare the mean conductance of the e→i synapses, which reflect the activity of the excitatory population. The lower panels show the calculated firing rate curves, together with an indication

Table 1 Synaptic parameters for the modeled networks.

Synaptic population		$\eta \rightarrow e$	e→e	e→i	i→e	i→i
Connection probability	p		0.5	0.5	0.5	0.5
Time constant	τ (ms)	45	45	34	45	34
Reversal potential	E_{syn} (mV)	50	50	50	-82	-82
Synaptic strengths						
1. Network w. type 1 cells	g_0 ($\mu\text{S}/\text{cm}^2$)	1.4	0.06	0.45	0.11	0.15
2. Strong feedback	g_0 ($\mu\text{S}/\text{cm}^2$)	5.4	0.06	0.45	8.0	0.15
3. Network w. type 2 cells	g_0 ($\mu\text{S}/\text{cm}^2$)	0.8	0.06	0.45	0.8	1.5
4. Type 1, variable E_k	g_0 ($\mu\text{S}/\text{cm}^2$)	1.4	0.30	0.45	1.65	0.15

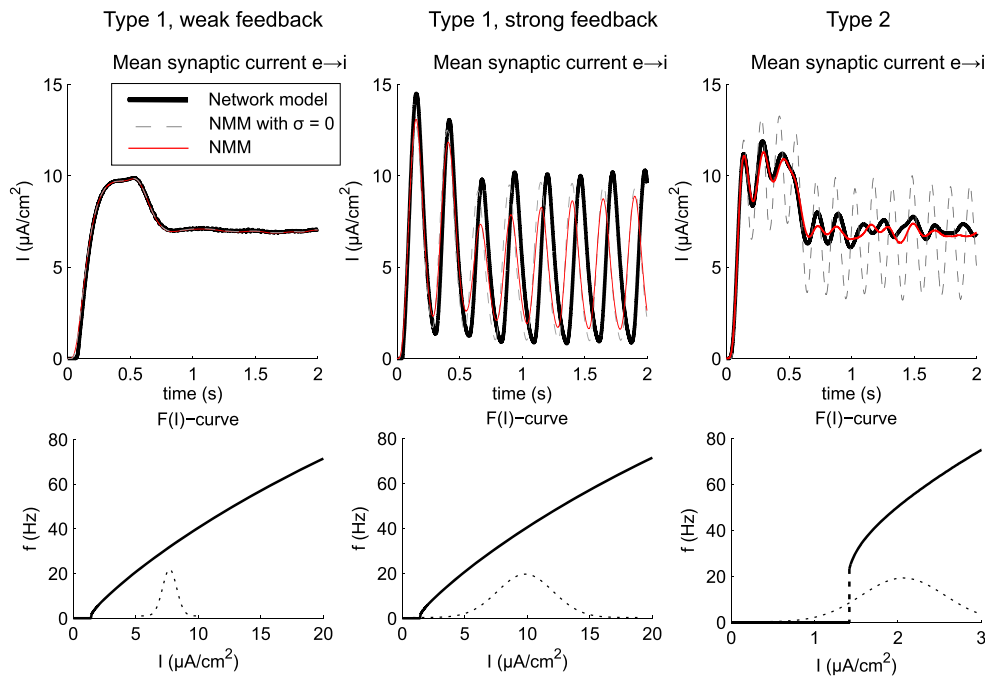


Fig. 7 Comparison of our NMM with a spiking network model, for the three different networks. Upper panels show the dynamics of the conductance of a single synaptic population ($e \rightarrow i$). These dynamics are representative for the other conductances. The reaction to a double step in input rate of the network model (*thick, black line*) is compared to that of our NMM (*thin red line*). To show the effect of neglecting the second moment of the input current distribution, the response of our model with the standard deviations set to zero is shown as well

(*dotted, gray line*). The bottom panels show the F(I)-curve of the neurons in the modeled networks. The Gaussian curves depict the typical width and position of the input distribution during the second half of the simulations (height is not scaled). Note that in the upper-right diagram a large discrepancy is observed between the network model and the 1st order approximation. The newly derived 2nd order model matches the data much better

of the instantaneous distribution of the input received by the excitatory neurons. More detailed results of the simulations, showing the conductances of all synaptic populations (mean and variance), as well as the firing rates of both neuronal populations (mean and variance) are presented in Appendix C. Figure 7 furthermore shows the effects of neglecting the second moment of the distribution. Namely, the dashed line shows the dynamics for a simulation where the variances were ignored, i.e. $\sigma_I = 0$.

In general, the behavior of the network model is well reproduced by the NMM. In all three simulations, the models are presented with a double step in external input rate. First, the conductance of the externally activated synapses rises (Fig. 6), which is followed by the firing rate of the excitatory population. This subsequently activates the excitatory synapses, followed by the inhibitory population. At $t = 0.5s$, the input rate is stepped down, which is subsequently followed by the synaptic conductances and firing rates.

The left panels show the simulations of type 1 cells with relatively weak feedback. In this network, the dynamics of the excitatory population are mainly determined by the external input and the dynamics of the inhibitory population are mainly determined by the firing rate of the excitatory

cells. The dynamics are very well reproduced. Also, the variances of the firing rates and synaptic conductances are accurately reproduced (Appendix B). The F(I)-curve of the type 1 neurons is relatively straight for frequencies above 10 Hz. Hence the sigmoidal function Equation (8) is almost equal to the F(I)-curve regardless of the variance in the input current. Neglecting the second moment of the input current distribution does hardly influence the dynamics of the populations.

We further tested our NMM by simulating the same network with strong feedback (center panels). Increasing the strength of the $i \rightarrow e$ synapses, first leads to the appearance of a resonance peak in the spectrum, i.e. spindles in the time domain (not shown). This is followed by the appearance of a limit cycle. The center panels show the dynamics where $g_{0,i,e}$ has been increased from 0.1 to 8 $\mu S/cm^2$. The input strength $g_{0,\eta}$ is increased from 1.4 to 5.4 $\mu S/cm^2$ to compensate for the inhibition. The NMM underestimates the amplitude of the oscillations, also in the resonating regime (not shown) and the time courses of the synaptic currents are more sinusoidal than those in the network model. However, the approximate frequency of the limit cycle, as well as the relative phases and amplitudes of the firing rates and synaptic currents of the two populations (Appendix C) are

well reproduced. Again, the neurons are operated on a part of the curve that is relatively flat, and neglecting the second moment of the input current distribution does not qualitatively affect the dynamics of the populations. In this case, we actually observe a slightly better numerical agreement when neglecting the second moment.

Finally, we tested whether our new NMM can also reproduce the behavior of a network of type 2 firing neurons (right panels). In this network, the width of the input current distribution has a larger influence on the dynamics, due to the step in the $F(I)$ -curve. Here, neglecting the second moment of the input current distribution leads to significantly different behavior. Advantageous for our approach is that the single cell dynamics have a negligibly small region of bistability. The oscillations of the synaptic currents (and firing rates, Appendix C) in the new NMM are less pronounced than in the spiking network, but the general behavior is very well reproduced. The mean of the firing rate is slightly underestimated, what in turn causes the standard deviation of the synaptic currents and firing rates to be underestimated. Considering that the network operates close to the thresholds of the neurons, where the standard deviation of the firing rates is very sensitive to the synaptic current distribution, the new NMM performs well.

5.1.1 Frequency spectrum

We investigated the frequency spectrum of the dynamics of the first simulation in more detail. Figure 8 shows a close-up of the dynamics of one of the synaptic currents and its frequency spectrum. The new NMM reproduces the low frequency part (< 20 Hz) of the firing rate signal very accurately.

The synaptic currents in the spiking network model show small oscillations in the frequency band around the modal firing rates of the populations. These oscillations are caused

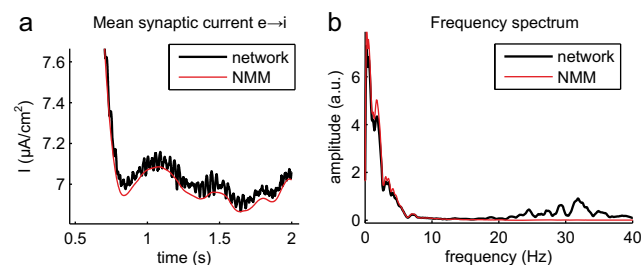


Fig. 8 Panel a shows a close up of the mean synaptic current (Fig. 7, upper left panel). The new NMM predicts the DC value accurately within 1 % error. Also, the low frequency oscillations observed in the network model are accurately reproduced. Panel b shows the corresponding frequency spectrum. The spectrum is accurately reproduced below 18 Hz. A broad peak is observed around 30 Hz, the mean firing rate, in the dynamics of the network model. As expected, this is not reproduced by the new NMM

by some of the neurons firing in phase. As expected, the NMM does not produce these oscillations, since neural mass models assume that phase effects are averaged out.

5.1.2 Relation of input and firing rate of the single cells

Now we will check how well the instantaneous input determines the firing rate of the single cells, as described by Equation (15). The actual firing rates observed in the spiking network model are compared to those predicted from the synaptic input the individual cells receive in Fig. 9. Panel a compares these for two randomly chosen (excitatory) cells in our first simulation. The firing rate is predicted accurately from the instantaneous synaptic conductances, even though the synaptic input fluctuates on a time scale similar to the firing rate rather than much slower. Panel b shows the mean of these rates for the entire populations. Even though the synaptic input predicts the firing rate for the single cells accurately, the firing rate of the population shows fluctuations around the predicted curve. This shows that the firing of the cells is to some extent synchronized. Even more pronounced synchronization is found during large amplitude limit cycles, shown in panel c. The firing rates of the populations in the network model exhibit a damped oscillation around the rates predicted from the input currents, especially clear for the inhibitory population. Panel d shows that the firing rates of both populations are systematically underestimated in the simulation of the network with type 2 cells. We found this was caused by the shunting effect of the inhibitory conductance, which was neglected in our NMM.

5.2 Dynamical transitions induced by extracellular potassium

The extracellular potassium concentration $[K]_e$ is tightly regulated in the brain, in order to maintain physiological neuronal functioning. Pathological increases in this concentration increase the excitability of neurons and can hence alter network dynamics. This may play an important role in spreading depression and epileptic seizures (Somjen 2004; Fröhlich et al. 2008). We demonstrate that our approach can easily be used to model the effects of such changes in single cell electrophysiology.

As example, we simulated a gradually increasing extracellular potassium concentration. In this simulation, $[K]_e$ was gradually increased from 4 to 16 mM. This corresponds to an increase of the potassium reversal potential E_k from approximately -95 to -60 mV (Fig. 10-b). Figure 10-c shows the $F(I)$ -curves for various values of E_k . Increasing extracellular potassium levels increases the neuronal excitability, i.e. the firing rates increase and the threshold current decreases. When E_k becomes larger than -75 mV,

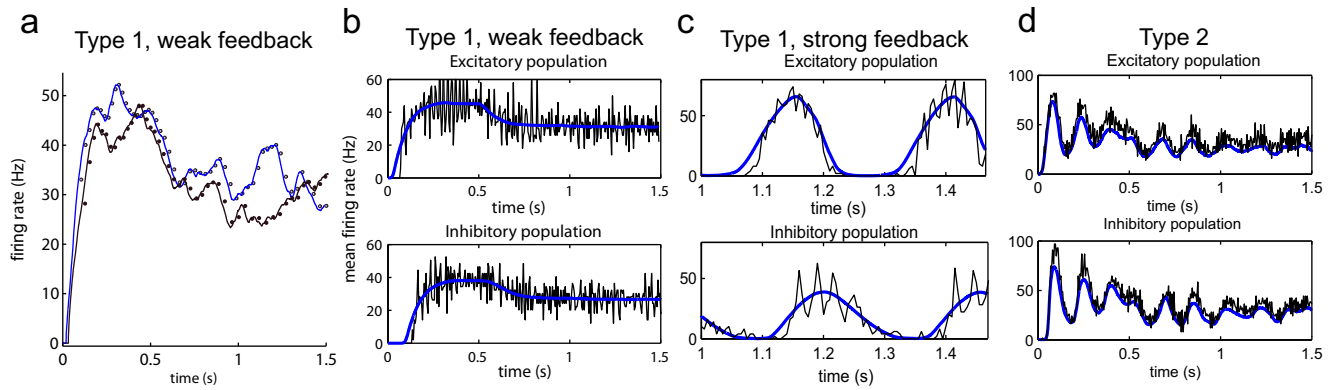


Fig. 9 Firing rates assumed from the synaptic input versus observed firing rates. Panel a shows the firing rates of two randomly chosen excitatory cells of type 1 with weak feedback. The full lines represent the firing rates calculated from the F(I)-curve and I(t) of the individual neurons. The dots are the spike rates determined from the recorded interspike interval. Panels b, c and d compare for the three networks the average firing rates for all neurons determined from the binned spike

times (*thin black line*) and the rates calculated from the input currents (*thick blue line*). Clearly visible are the fluctuations of the population rate around the calculated rate (**b**), oscillations around the calculated rate during large amplitude limit cycles (c, note the different time scale) and a general underestimation of the firing rate by 10 – 20 % for the simulation with type 2 cells (**d**)

the threshold current even becomes negative, i.e. the neurons generate action potentials unless they are inhibited.

Figure 10-a shows the resulting dynamics of the two populations (mean firing rates). Increasing $[K]_e$ to 6 mM ($t \approx 4s$) makes both the excitatory and inhibitory cells more excitable. The net effect here is an increased firing rate of the inhibitory population, which slightly suppresses the

excitatory activity. Further increasing $[K]_e$ increases the activity of the inhibitory cells even more. When $[K]_e$ is increased above 8 mM, ($t \approx 8s$), the system becomes unstable and a limit cycle appears. This cycle grows in amplitude when $[K]_e$ is increased further. The firing rates of both populations oscillate with large amplitudes and the cells in the excitatory population show synchronized bursts of firing.

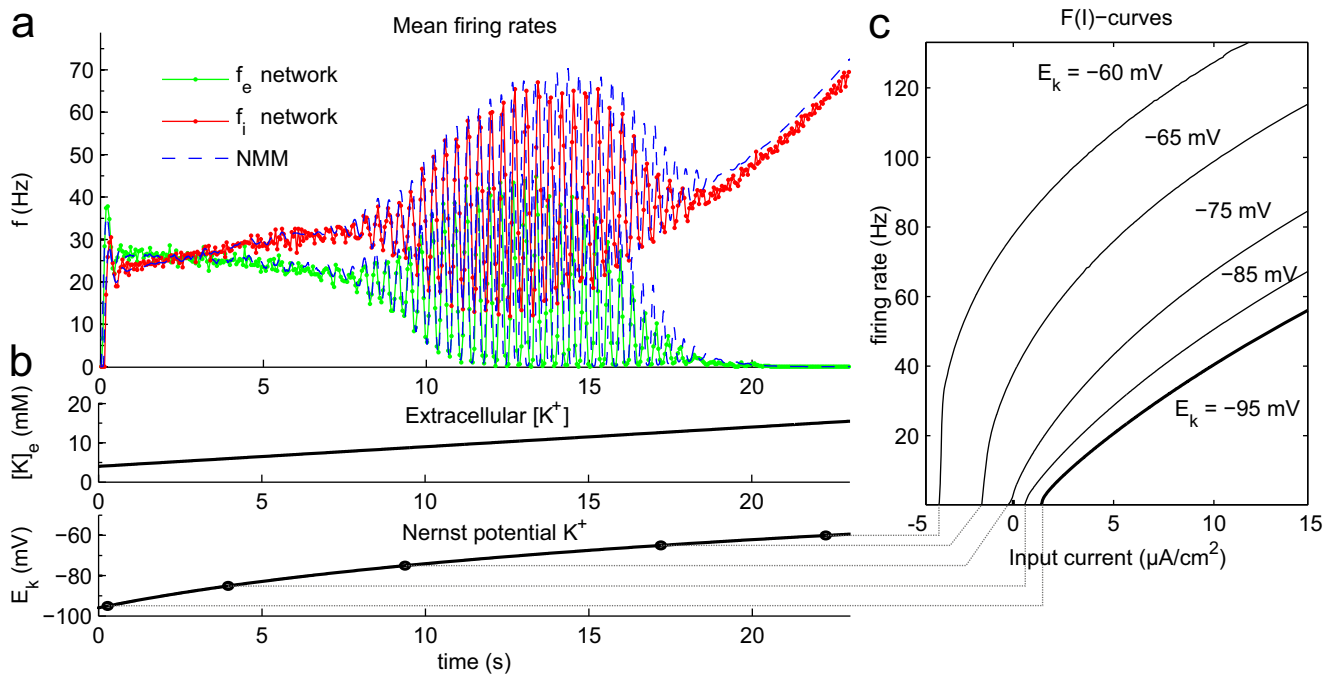


Fig. 10 Population dynamics during steadily increased extracellular potassium concentrations. Panel a shows the mean of the firing rates of both populations during the process. The resulting dynamics of our NMM (*blue dashed lines*) are compared to those of the spiking

network model (*full lines with dots*). Panel b shows the concentration $[K]_e$ and corresponding Nernst potential E_k as a function of time. Panel c shows how the F(I)-curve correspondingly changes

When the inhibitory cells become even more active due to the high E_k , the activity of the excitatory cells is completely suppressed ($t \approx 18$ s). Again, our neural mass model excellently reproduces the dynamics and transitions of the firing rates in the spiking network model. Also quantitatively, the amplitude and frequency of the fluctuations and limit cycles are reproduced very well. The accuracy gets lower as the inhibitory input to the populations becomes stronger, typically after $t = 12$ s. As discussed previously, this results from neglecting shunting by the inhibitory conductance in our NMM.

This result shows that changes and transitions of network dynamics induced by varying parameters of the single cells can be quantitatively reproduced and investigated with our neural mass model.

6 Discussion

Neural mass models are designed for modeling macroscopic electrical activity of the brain. Cortical neural dynamics, as in part reflected by the EEG, are modulated by various conditions, ranging from anesthesia, the use of central acting drugs and hypoxia/ischemia. Modes of action include interactions with ligand-gated and voltage-gated ion channels, energy dependent ion pumps, and synaptic failure. In existing neural mass models only the synaptic response is explicitly modeled, which allows only for investigating neural dynamics during altered synaptic functioning. To extend these investigations to altered electrophysiological conditions, here we introduced a neural mass model explicitly including single cell dynamics, with a sigmoid function derived from the single cell F(I)-curve.

Using the F(I)-curve as link between single cell and macroscopic dynamics has several distinct advantages. It can easily be calculated numerically from a physiological plausible model, without reduction or analysis of the dynamics. The curve is a familiar function for most and the influence of pathologies on its shape can be understood intuitively. It carries information on excitability, sensitivity and maximum firing rates. Furthermore, depolarization block of the cells, important for example during certain types of epilepsy (Ziburkus et al. 2006), is naturally included in the F(I)-curve.

The usual techniques can be used to analyze the dynamics of the model for changes in the F(I)-curve. For example, the dependency of the steady state firing rates on E_K can be calculated from an analysis of the nullclines of the system, and linearizing the NMM around a fixed point and calculating the transfer function between the input and the synaptic conductance yields the power spectrum.

The approach presented for constructing the sigmoidal function in our NMM can be used to adapt existing neural

mass models as well, for example the Jansen en Rit model (Jansen and Rit 1995) or the Robinson model (Robinson et al. 2001). This allows to investigate the effects of altered single cell dynamics on the EEG signals predicted by these models.

The new model was validated by quantitatively comparing it with a network of spiking neurons, representing neural tissue with pyramidal cells and interneurons. This spiking network model consisted of both excitatory and inhibitory Hodgkin-Huxley neurons. The newly derived NMM was shown to describe the synaptic activations and the population firing rates accurately. We also illustrated the use of our neural mass model for simulating pathological conditions by modeling increased extracellular potassium.

We will now first discuss this example in some more detail, followed by some restrictions on our approach. Then we discuss possibilities for extensions of our model such as including unreliability of synaptic transmission. Furthermore, we discuss phase synchronization and how this affects the frequency spectrum of macroscopic measurements. Finally we will deliberate on similar investigations by others, and how these complement this work.

6.1 Modeling pathophysiology

Our NMM allows for quantitatively investigating the influence of parameters of the single cell model on the network activity. This is not possible in traditional NMM's. To illustrate the possibilities of our NMM, we simulated network dynamics for an increasing extracellular potassium concentration. In reality, the dynamics of extracellular potassium in the brain are coupled to, and largely determined by, the neuronal activity. However, the potassium dynamics are typically on a slower time scale (seconds) than the dynamics of the neural activity, which allows us to separate them, and investigate the neural dynamics as a function of $[K]_e$.

Our simulations show that upon increasing $[K]_e$, eventually the system's equilibrium point loses stability, giving rise to large amplitude, limit cycle activity of the populations. In the network model, synchronized bursts of the excitatory neurons are observed during these oscillations (not shown). We speculate that local disturbance of potassium homeostasis and resulting limit cycle activity of localized populations may play a role in the generation of epileptic microseizures found at the onset of electrographic seizures (Schevon et al. 2008; Stead et al. 2010). Interestingly, in the case we simulated, the limit cycle activity is induced by increased inhibition of the excitatory population and could be prevented by either stimulating the excitatory neurons or inhibiting the inhibitory population. Naturally, the resulting dynamics depend on the various parameters of the system, and the strengths of the synaptic connections in particular. Due to its relatively low dimensionality, our NMM allows

for bifurcation analysis, allowing to investigate these dependencies in detail. This falls outside the scope of this paper, however.

Other changes resulting from pathology or drug interactions can be investigated with our NMM as well. For example, altering conductances or rate constants of the voltage gated channels in the single cell model would mimic channel mutations or channel blockers.

6.2 Valid parameter ranges

The main assumption for neural mass modeling in general is that a neuron's input current consists of contributions from many action potentials, i.e. $N_{\text{syn},xy} f_x \tau_{xy} \gg 1$. This is the case for typical physiological parameters in cortex, e.g. $N = 2000$, $f = 4$ Hz and $\tau = 50$ ms, for which a cell receives 400 action potentials during a synaptic integration time.

A second assumption made in our derivation is that the synaptic input currents instantaneously determine the firing rate. We have shown this is the case when the synapses fluctuate on a time scale slower than or similar to the spike rate, i.e. $\tau_{xy} \gtrsim 1/f_y$. Hence, dynamics involving low spike rates or very short somatic PSP's are not modeled accurately. By assuming the F(I)-curve characterizes the instantaneous firing rate, action potentials resulting from subthreshold fluctuations were neglected. Further work is needed to determine if low firing rates can be modeled by incorporating the finite firing rates for fluctuating or noisy subthreshold input into the F(I)-curve, as for example done in (Galtier and Touboul 2013). This would be necessary depending on which brain area is modeled. While cortical neurons typically have low average firing rates, rates are higher in other brain structures.

To test our model, we have chosen synaptic time constants of 45 and 34 ms for the response by excitatory and inhibitory cells respectively. This number may seem high when compared with the synaptic time constants used by e.g. Liley et al. (3 and 15 s for excitatory and inhibitory synapses, respectively). However, Liley et al. filter the synaptic responses with an additional linear equation representing the membrane, for which they obtain time constants of 90 and 65 ms to reproduce experimental EEG's. We have based our choice of the time constants on these numbers to obtain similar synaptic integration times. Alternatively, we could have used a ball-and-stick single neuron model rather than a point model. In that case, a faster time constant could have been chosen for the synaptic response, that is subsequently filtered with a slower response of the dendrite. Similarly, a bi-exponential function could be used with a faster time constant for the rise time.

We have shown that our NMM still fairly accurately reproduces the dynamics of the spiking network, even

when some of the assumptions made in deriving the model are hardly valid. For example, the time constants of the synapses do not need to be much longer than the interspike intervals, and also with considerable shunting by the inhibitory synaptic conductance the qualitative dynamics are still reproduced. When using the NMM for analyzing network activity in parameter ranges where the assumptions may not be valid, we recommend to validate the dynamics predicted by the model with a network of spiking neurons.

6.3 Modeling additional effects

The inhomogeneity of the single cell parameters was chosen such that it could be described as an additional input current, i.e. a shift in the F(I)-curve for each neuron. In the case of heterogeneous properties of the neurons that do more than shift the F(I)-curve, two curves can be determined from the single cell description. The average F(I)-curve of the population, as well as the σ_{fp}^2 (I)-curve, the variance of the firing rate over the population for the same I. This term can be added to variance of the firing rate Equation (6).

We have assumed reliable synapses, that release a quantum of neurotransmitter with every action potential. Actual synapses are known to be quite unreliable, and typically fail to activate > 50 % upon receiving an action potential (Allen and Stevens 1994). We did not investigate unreliability, but this can be included in the model as an additional term in the variance.

Furthermore, we assumed that the inhibitory conductance can effectively be subtracted from the excitatory conductance Equation (16). However, when the inhibitory synaptic current is large compared to the net input current, we found that it also shunts the gated currents, reducing the spike rate. This notably affected the simulation with the type 2 cells, that received a relatively large amount of inhibitory input. Firing rates based on the net synaptic input were underestimated by 10 – 20 %. To include the shunting effect of the inhibitory input as well, equation 16 could be adapted with an extra non-linear term.

Finally, we assumed the neurons in our population have a simple F(I)-curve, and do not exhibit, for example, bistability or bursting. Mathematical techniques are being investigated to include bursting (Pa et al. 2008; Visser and Van Gils 2014) or bistability (Galtier and Touboul 2013) into neural mass models. These techniques can be applied to our model as well.

6.4 Phase synchronization

Because the output of a neuron consists of a train of action potentials, the postsynaptic conductance it induces fluctuates even when firing at a constant rate. In first order

approximation, these fluctuations are sinusoidal oscillations. One of the assumptions in neural mass modeling is that the spike timings of neurons within a population are unsynchronized and therefore these oscillations are assumed to cancel out when considering a large number of synapses. When, contrary to this assumption, there is synchronization of the spike timings, oscillations do appear in the total postsynaptic synaptic currents in the frequency range around the modal firing frequency of the presynaptic population. These oscillations subsequently appear in the spectra of macroscopic measurements such as the EEG. Therefore, we discuss these oscillations observed in the network model and how the dynamics of the neural mass model in this frequency range deviate.

The first cause for these oscillations is no synchronization, but rather a finite size effect. Randomly distributed phases of a finite number of firing neurons do not completely cancel, which results in oscillations in the total synaptic inputs of smaller networks. However, the relative amplitude of these oscillations declines as $1/\sqrt{N}$. This is negligible for a large number of cells N in a population. This effect is a limitation of the (small) network model used for validation, rather than of the NMM.

Furthermore, two different mechanisms cause synchronization. The first mechanism, exemplified in Fig. 9-c, is a sudden increase in the input current of a population (Wilson and Cowan 1972). A population density approach using the time-since-last-spike can accurately model this phenomenon for current based models (Chizhov and Graham 2007). Furthermore, the output lags, for sudden changes in input current. The approach of Ostojic and Brunel using a frequency dependent lag (Ostojic and Brunel 2011), can be used to investigate this. This lag and synchronization are transient phenomena (Wilson and Cowan 1972), and therefore not of interest when predicting the frequency spectra of ongoing neural activity.

The second mechanism is the tendency of neurons to synchronize with modulations in their input. A population's firing rate hence amplifies modulations in the input at frequencies similar to the modal firing rate. Shriki et al. (Shriki et al. 2003) have shown this effect can be modeled by filtering the input current with a (phenomenological) second order resonance filter before calculating the firing rate. This amplification is expected to be larger for two coupled populations than for the single population described by them. The tendency to synchronize also occurs in our simulations of the network model. We did not investigate how this synchronization scales with N_{syn} and $\text{var}(N_{\text{syn}})$, because it was not possible in our implementation to uncouple the relevant parameters for this mechanism (number of cells and synaptic connections, fluctuations in external input and width of synaptic current distributions).

In summary, our neural mass model does per definition not show any effects of phase synchronization within a population. These have been shown to occur, also in large populations of neurons, and result in oscillations at frequencies near the modal firing rates. This should be kept in mind when interpreting the dynamics of any neural mass model. In our simulations, synchronization did not affect the dynamics at lower frequencies. When the frequency bands around the modal firing rates are of interest, several available techniques that can be used to investigate phase synchronization were discussed.

6.5 Complementary work

When our NMM is operated in a regime where the F(I)-curves are relatively straight, the variance of the synaptic input has little influence on the average firing rate and our model can be greatly simplified. In that case, the F(I)-curve can directly be used as sigmoid, without keeping track of the variances, reducing our approach to that of Shriki et al. (Shriki et al. 2003) who consider only the average input in their analysis of the network activity.

Hutt (Hutt 2012) derived a sigmoidal function in a similar manner as Wilson and Cowan (Wilson and Cowan 1972), but included the firing rate curve, rather than assuming all-or-none firing neurons. However, he considered the variances of the state of the neurons to be given, while we derived these from the statistics of the recurrent synaptic input.

Deco et al. (Deco et al. 2008) discuss a more profound method for deriving a NMM, starting from ensemble density models. This method, however, assumes the population dynamics can be described with a diffusion approximation. This is not the case in our networks, because the cells receive heterogeneous input and hence the state of the tonically firing cells is strongly correlated with their input. To model low firing rates, we recommend to adapt such an approach as described by Deco et al. by taking this heterogeneity into account. This allows modeling of pathological populations with relatively low firing rates, for which the NMM we presented is not valid.

The approach of Faugeras et al. (Faugeras et al. 2009) describes the dynamics of a network of synaptically connected neurons. They show existence and uniqueness of the solution to a mean-field equation. It considers the same system as we do, i.e. synaptically connected cells that fire instantaneously depending on their input, but is not concerned with the derivation of a specific sigmoid function. Further work describes the effects of noise in such a system (Touboul et al. 2012). Our derivation of the sigmoid could be combined with their more elaborate approach to the statistics of the network. This would allow for a rigorous investigation of the parameter regimes in which the

dynamics of the network model converge to those of the neural mass equations, i.e. where the mean and variance alone provide an adequate description of the firing rate dynamics. This is not always the case, for example in networks that exhibit avalanches or synchronized firing. Other work from this group (Baladron et al. 2012) describes networks of Fitzhugh-Nagumo and Hodgkin-Huxley neurons. The obtained (McKean-Vlasov-)Fokker-Planck equations describing the state density of the populations are very accurate, but unfortunately also very expensive computationally. In very recent work, (Galtier and Touboul 2013) describe an approach for modeling networks of spiking neuron models, and also specifically address the HH neuron. Similar to us, they use a hybrid approach, in which the response of the single cell model is calculated numerically. Instead of action potentials and firing rates, they consider the time-averaged membrane potential of the cells, and assume synapses that react linearly to this voltage. To obtain the sigmoid function from a smoothed single cell response, we considered the variance of (slowly varying) synaptic inputs over the population and neglected noise. In contrast, they reduced this variance to zero, but considered the input to be stochastic noise. As discussed in section 6.2, this noise drives subthreshold oscillations, resulting in non-zero firing rates at subthreshold input. These need to be considered, in addition to the variance, when modeling low population firing rates. However, it should be kept in mind that these input fluctuations or noise are largely induced by synaptic activity (Manwani and Koch 1999), and suitable expressions for the noise need to be obtained.

7 Conclusion

We have presented a new neural mass model that is fully derived from physiological expressions. It was shown how a sigmoidal function can be calculated from the F(I)-curves of the single cells and the variances of the firing rates. Additionally, we presented expressions for the dynamics of the variances of the neuronal firing rates and synaptic conductances.

We showed this model excellently reproduces the dynamics observed in a network of heterogeneously coupled excitatory and inhibitory HH-neurons. The time courses of the means and standard deviations of both the firing rates and the synaptic conductances are all described accurately. Furthermore, it was discussed that the model is valid as long as the synaptic conductances fluctuate on a time scale similar to or slower than the neurons' spike rates, and the modal firing rates are higher than the frequencies of the dynamics of interest.

Besides yielding the variance of the firing rates and input currents in the populations, our approach allows for inves-

tigating how alterations of the single cell dynamics affect the macroscopic activity. The firing rate curve of the single cell serves as link between the two. For pathologically and pharmacologically induced changes this curve can be calculated directly with a biophysical single cell model, without the need for analytically reducing the model to a simpler form first. We demonstrated this for an increased extracellular potassium concentrations. A wide range of alterations of the single cell dynamics, for example by channel blockers, can be modeled in the same way.

Conflict of interest The authors declare that they have no conflict of interest.

Acknowledgements This work was financially supported by Ministerie van Economische Zaken, Provincie Overijssel and Provincie Gelderland through the ViPBrainNetworks project. The funders had no role in study design, data collection and analysis, decision to publish, or preparation of the manuscript.

Appendix A: Distribution of the synaptic input dynamics and distribution of the synaptic input in a network of spiking cells

A network with excitatory and inhibitory neurons, contains four sets of synaptic connections ($e \rightarrow e$, $e \rightarrow i$, $i \rightarrow e$ and $i \rightarrow i$). We describe the total synaptic conductance G_n induced by one of these sets on a postsynaptic neuron n (see Fig. 11). First, the distribution of G is derived from a synaptic connection matrix. We denote the number of cells in the presynaptic population with M , and that in the postsynaptic one with N . This yields a maximum of $N \times M$ synapses in the set. The presence and strength of the synaptic connections is described with an $N \times M$ matrix W . $W_{n,m} = 1$ denotes a synaptic connection from cell m to n of average weight, while 0 stands for no connection. This system is equal to that analyzed by Faugeras et al. (Faugeras et al. 2009), however we do not constrain our analysis to a normal distribution of $W_{n,m}$.

We assume the states of the synapses originating from the same presynaptic cell m are all equal, except for their weight. They are therefore described with the same variable $g_m(t)$. The conductance of the synapse $g_m(t)$ is described as the convolution of the impulse response H with the spike rate $f_m(t)$ of cell m :

$$g_m(t) = H * f_m(t). \tag{25}$$

The total synaptic conductance G_n of cell n induced by one presynaptic population, is calculated as the linear sum of all synapses, using the connection matrix:

$$G_n(t) = \sum_m W_{n,m} g_m(t). \tag{26}$$

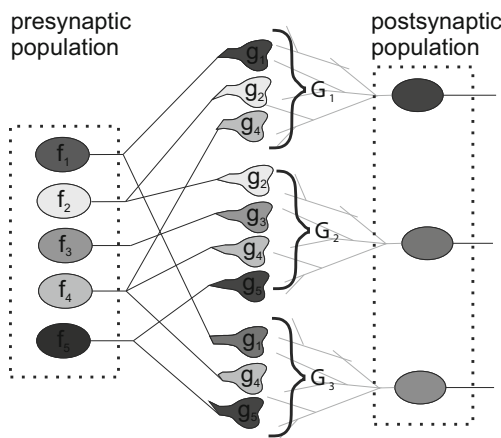


Fig. 11 Sketch of the synaptic variables. One synaptic population is shown, with presynaptic single cell firing rates f_m , synaptic conductances g_m and summed synaptic conductances G_n

Assuming the firing rates and synaptic strengths are uncorrelated, and defining the weighted number of connections neuron n receives as

$$N_{\text{syn},n} := \sum_m W_{n,m}, \tag{27}$$

the mean of the total synaptic conductance \bar{G} is readily calculated:

$$\bar{G}(t) = \bar{N}_{\text{syn}} \bar{g}(t) = \bar{N}_{\text{syn}} H * \bar{f}(t), \tag{28}$$

using bars to denote the mean values.

This derivation may seem an unnecessarily elaborate way of obtaining the familiar Eq. (28), but it sets the stage for deriving the variance of G .

To calculate the variance of G_n Eq. (26) over the N postsynaptic cells, the terms $W_{n,m}$ and g_m are written as their mean plus a deviation:

$$\bar{W}_n := \frac{1}{M} \sum_m W_{n,m} \tag{29}$$

$$\Delta W_{n,m} := W_{n,m} - \bar{W}_n \tag{30}$$

and similar for g . With these expressions, the variance of G_n Eq. (26) is calculated:

$$\sigma_G^2 := \text{var}_n(G_n) = \text{var}_n(\sum_m W_{n,m} g_m) \tag{31}$$

$$= \text{var}_n(\sum_m (\bar{W}_n + \Delta W_{n,m})(\bar{g} + \Delta g_m)) \tag{32}$$

$$= \text{var}_n\left(\bar{g} \sum_m \Delta W_{n,m} + \bar{W}_n \sum_m \Delta g_m + M \bar{W}_n \bar{g} + \sum_m \Delta W_{n,m} \Delta g_m\right). \tag{33}$$

The subscript n denotes the variance is calculated over n . The first two terms are zero, since the sums over the deltas are per definition zero. Hence,

$$\sigma_G^2 = \text{var}_n(M \bar{W}_n \bar{g} + \sum_m \Delta W_{n,m} \Delta g_m) \tag{34}$$

Assuming the synaptic weights and synaptic activations are uncorrelated and using the standard rules for the variance of products and sums:

$$\sigma_G^2 = \text{var}(M \bar{W}_n) \bar{g}^2 + (\sum_m \text{var}_n(W_{n,m})) \text{var}_m(g_m), \tag{35}$$

noting that $M \bar{W} = N_{\text{syn}}$ (equation 27), $\text{var}_m(g_m) \equiv \sigma_g^2$ and defining

$$N'_{\text{syn}} := \sum_m \text{var}_n(\Delta W_{n,m}), \tag{36}$$

this is results in:

$$\sigma_G^2 = \text{var}(N_{\text{syn}}) \bar{g}^2 + N'_{\text{syn}} \sigma_g^2. \tag{37}$$

The first term is the variance due to differences in the weighted number of synaptic connections N_{syn} received by the cells. The second term is the variance due to different synaptic activations caused by differences in presynaptic spike rates. N'_{syn} can be interpreted as the average number of connections a postsynaptic neuron does not share with a random other cell of its population. For example, in the case where all cells are connected with probability p it is equal to $Mp - Mp^2$, where Mp is equal to the average number of connections per neuron, and Mp^2 the average number of connections shared with another neuron. Note that these expressions do not require the number of synapses to approach infinity.

Now the task to describe the mean and variance of $g(t)$ is left. To calculate σ_g over the individual synapses, we need to make some assumptions on the distribution of the spikes in the input. Amit and Brunel calculated this variance in the steady state, assuming Poisson (shot noise) statistics (Amit and Brunel 1997). We will show a similar approach can be used for dynamic input and describe statistics for periodically generated action potentials, i.e. with regular intervals. These describe the firing rates observed in our spiking network model better.

There is a fundamental difference between calculating the distribution of the conductance induced by a Poisson process or by a periodical process. The conductance of a synapse receiving action potentials generated by a Poisson process with a known rate, is a stochastic signal. In contrast, the conductance of a synapse receiving action potentials periodically at a known rate is deterministic (assuming the synaptic integration smooths the input sufficiently, such that the phase of the input is irrelevant). Therefore, the variance of the synaptic conductances is induced by the variance of the firing rates themselves, rather than by the realization of the spike generation process. We calculate this variance now for time dependent firing rates.

The firing rates $f(t)$ are considered to be distributed over the presynaptic neurons, with mean $\bar{f}(t)$ and standard deviation $\sigma_f(t)$. We consider the inputs to be smooth continuous functions (rates) rather than delta pulse trains, as is common in neural mass modeling. The mean of the synaptic activation is trivial to calculate from Equation (25):

$$\bar{g} \equiv \langle g \rangle = \langle H * f \rangle = H * \bar{f} \tag{38}$$

where the brackets denote the expectancy.

To calculate the variance of g , we use hats to denote the deviation from the expectancy of f and g , i.e.

$$\hat{g} := g - \bar{g}, \tag{39}$$

and explicitly write the convolutions as integrals:

$$\sigma_g^2 \equiv \langle \hat{g}^2 \rangle = \langle (H * \hat{f}(t))^2 \rangle \tag{40}$$

$$= \left\langle \left(\int_0^\infty \hat{f}(t-u)H(u)du \right)^2 \right\rangle \tag{41}$$

$$= \int_0^\infty \int_0^\infty \langle \hat{f}(t-u)\hat{f}(t-u') \rangle H(u)H(u')dud u' \tag{42}$$

The expectancy is replaced by the (auto)correlation coefficient C_{ac} :

$$C_{ac}(x_1, x_2) := \frac{\langle x_1 x_2 \rangle}{\sigma_{x_1} \sigma_{x_2}} \tag{43}$$

$$\sigma_g^2 = \int_0^\infty \int_0^\infty C_{ac}(\hat{f}(t-u), \hat{f}(t-u')) \times \sigma_f(t-u)\sigma_f(t-u')H(u)H(u')dud u' \tag{44}$$

In our simulations of spiking networks it was observed that \hat{f} is highly correlated with itself over periods much longer than the duration of H , i.e. cells tend to fire faster or slower than the population average over longer periods of time. In that case $C_{ac} \approx 1$ and the right hand side of Equation (44) is equal to the squared convolution with the variance (c.f. Equations (40-42)),

$$\sigma_g(t) \approx H * \sigma_f(t), \tag{45}$$

which is used for our simulations.

For cases where \hat{f} does fluctuate faster (typically when $\text{var}(N_{\text{syn}})$ is low), Equation (44) can be simplified in another way. It is reasonable to assume the autocorrelation coefficient depends only on the time difference $u - u'$, while furthermore σ_f fluctuates slowly compared to the synaptic time constant. In that case, the autocorrelation coefficient can be effectively replaced with a correction constant C between 0 and 1. The expression for σ_g becomes:

$$\sigma_g(t) = C H * \sigma_f(t), \tag{46}$$

where

$$C = \frac{\int_0^\infty \int_0^\infty \exp(C_{ac}(u-u'))\sigma_f(t-u)\sigma_f(t-u')H(u)H(u')dud u'}{\left(\int_0^\infty H(u)du\right)^2}. \tag{47}$$

However, deriving a closed expression for the autocorrelation coefficient $C_{ac}(u - u')$ in a recurring network is complicated and outside the scope of this work.

Fig. 12 Comparison of our new NMM with a detailed network model. The reaction to a double step in input rate of the network model (full lines and dots) is compared to that of the NMM (blue dashed lines). The mean and standard deviation of three synaptic currents are displayed, as well as those of the firing rates of the excitatory and inhibitory populations

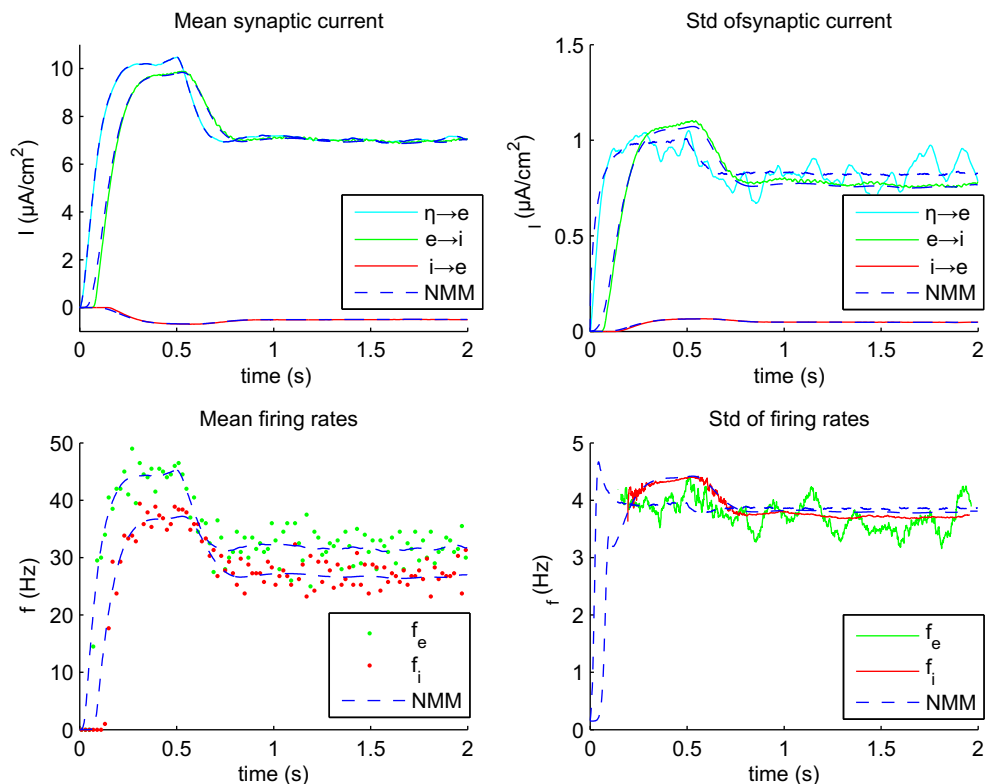


Fig. 13 Simulations of a network with strong feedback. The reaction to a double step in input rate of the new NMM (blue dashed lines) is compared to that of the network model (full lines and dots). The mean and standard deviation of three synaptic currents are displayed, as well as the firing rates of the excitatory and inhibitory populations. The standard deviations of the firing rates of the network model are not shown since they are dominated by artifacts

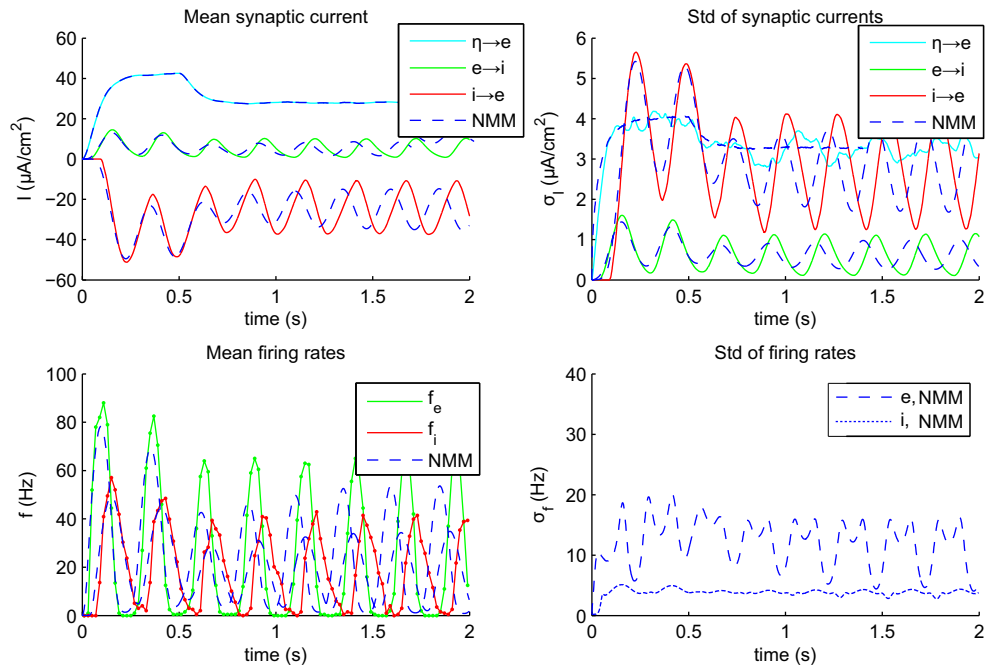
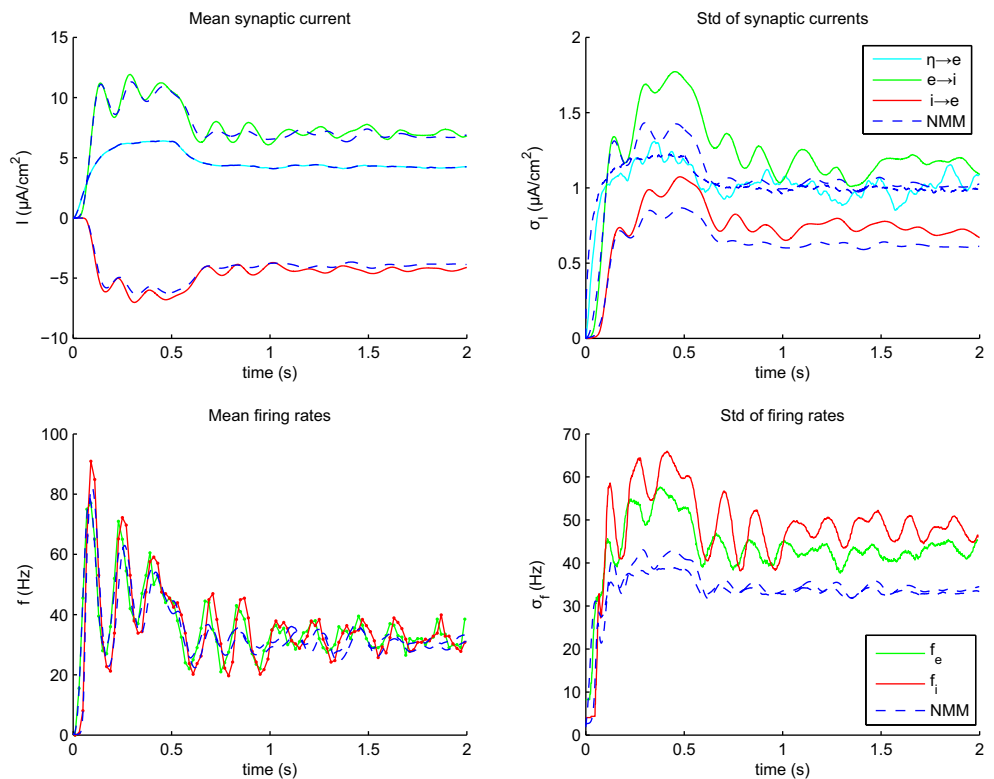


Fig. 14 The dynamics of two populations of type 2 spiking neurons. The reaction to a double step in input rate of the NMM (blue dashed lines) is compared to that of the network model (full lines). The mean and standard deviation of three synaptic currents are displayed, as well as those of the firing rates of the excitatory and inhibitory populations



Appendix B: Approximating a synaptic conductance with a constant current

We show how a synaptically induced (excitatory) current can be approximated with a constant input. This approach can be easily extended to include a second (inhibitory) conductance as well. First, we write the dynamics of a Hodgkin-Huxley (HH) model with the added synaptic conductance as:

$$C \frac{dV}{dt} = I_{\text{HH}}(t) + g_{\text{syn}}(E_{\text{syn}} - V(t)) \quad (48)$$

$$= I_{\text{HH}}(t) + \underbrace{g_{\text{syn}}(E_{\text{syn}} - V^*)}_{\text{constant current}} + \underbrace{g_{\text{syn}}(V^* - V(t))}_{\text{shunt}} \quad (49)$$

$$\approx I_{\text{HH}}(t) + g_{\text{syn}}(E_{\text{syn}} - V^*) \quad (50)$$

Here I_{HH} is the sum of all gated and leak currents in the HH model, g_{syn} is the synaptic conductance and E_{syn} the reversal potential of the synapse. The synaptic current was split in a constant current and a leak current or shunt. This distinction is artificial and therefore V^* is an arbitrary voltage, which we are free to choose. Our aim is to choose it such, that neglecting the shunting term changes the firing rate minimally. For example, when the (type 1) HH neuron is firing action potentials, the region around the threshold voltage V_{th} is traversed relatively slowly, due to the ghost of the saddle-node bifurcation (Izhikevich 2007). The time taken to traverse this region largely determines the firing rate. Therefore, for continuously firing HH neurons, an accurate approximation for the firing rate is obtained when V^* is set to V_{th} , such that the shunting term is small in that region.

Choosing an optimal V^* minimizes the error in the approximation, but does not guarantee that it is accurate. In order for the approximation to be accurate, the synaptic conductance should be small compared to the total (leak and gated) conductance. For our single cell models, the approximation was empirically validated.

Note that the optimal value for V^* depends on the specific single cell model used. However, we found that also the firing rate of our type 2 neuron was approximated reasonably when V^* was set to V_{th} , with an accuracy depending on the relative magnitude of the inhibitory conductance.

Appendix C: Detailed results

We show the results of the simulated networks, as described in the main body of the paper, in more detail. Results are shown for networks of type 1 neurons with weak feedback (Fig. 12), with strong feedback (Fig. 13) and type 2 neurons (Fig. 14). The NMM model describes the dynamics of the network of neurons very well, both for the synaptic conductances (mean and variance) and the firing rates (mean

and variance). The fluctuations in the standard deviations are caused by the small size of the modeled network. These are stochastic in nature and hence are not reproduced by the NMM.

References

- Allen, C., & Stevens, C.F. (1994). An evaluation of causes for unreliability of synaptic transmission. *Proceedings National Academy Science USA*, 383(10), 380–10.
- Amit, D., & Brunel, N. (1997). Dynamics of a recurrent network of spiking neurons before and following learning Network Computation in Neural Systems.
- Baladron, J., Fiasoli, D., Faugeras, O., Touboul, J. (2012). Mean-field description and propagation of chaos in networks of Hodgkin-Huxley and Fitzhugh-Nagumo neurons. *Journal Mathematics Neuroscience*, 2(1), 10. doi:10.1186/2190-8567-2-10.
- Bazhenov, M., Timofeev, I., Fröhlich, F., Sejnowski, T.J. (2008). Cellular and network mechanisms of electrographic seizures. *Drug Discovery Today Dis Models*, 5(1), 45–57. doi:10.1016/j.ddmod.2008.07.005.
- Bhattacharya, B.S., Coyle, D., Maguire, L.P. (2011). A thalamo-cortico-thalamic neural mass model to study alpha rhythms in Alzheimer's disease. *Neural networks : the official journal of the International Neural Network Society*, 24(6), 631–45. doi:10.1016/j.neunet.2011.02.009.
- Chizhov, A., & Graham, L. (2007). Population model of hippocampal pyramidal neurons, linking a refractory density approach to conductance-based neurons. *Physical Review E*, 75(1)(011), 924. doi:10.1103/PhysRevE.75.011924.
- De Schutter, E. (2010). Computational Modeling Methods for Neuroscientists. *Mit Press, chap. 6*. URL http://books.google.nl/books/about/Computational_Modeling_Methods_for_Neuro.html?id=20RvPgAACAAJ&pgis=1.
- Deco, G., Jirsa, V.K., Pa, R., Robinson, J., Breakspear, M., Friston, K. (2008). The dynamic brain: from spiking neurons to neural masses and cortical fields. *PLoS computational biology*, 4(8)(e1000), 092. doi:10.1371/journal.pcbi.1000092.
- Dreier, J.P. (2011). The role of spreading depression, spreading depolarization and spreading ischemia in neurological disease. *Nature medicine*, 17(4), 439–47. doi:10.1038/nm.2333.
- Faugeras, O., Touboul, J., Cessac, B. (2009). A constructive mean-field analysis of multi-population neural networks with random synaptic weights and stochastic inputs. *Frontiers in computational neuroscience*, 3(February), 1. doi:10.3389/neuro.10.001.2009.
- Fröhlich, F., Bazhenov, M., Iragui-Madoz, V., Sejnowski, T.J. (2008). Potassium dynamics in the epileptic cortex: new insights on an old topic. *Neuroscientist*, 14(5), 422–433. doi:10.1177/1073858408317955.
- Galtier, M.N., & Touboul, J. (2013). Macroscopic equations governing noisy spiking neuronal populations with linear synapses. *PLoS One*, 8(11)(e78), 917. doi:10.1371/journal.pone.0078917.
- Grefkes, C., & Fink, G.R. (2011). Reorganization of cerebral networks after stroke: new insights from neuroimaging with connectivity approaches. *Brain : a journal of neurology*, 134(Pt 5), 1264–76. doi:10.1093/brain/awr033.
- Hindriks, R., & Putten, v.an.M.JaM. (2012). Meanfield modeling of propofol-induced changes in spontaneous EEG rhythms. *NeuroImage*, 60(4), 2323–34. doi:10.1016/j.neuroimage.2012.02.042.

- Hines, M.L., Morse, T., Migliore, M., Carnevale, N.T., Shepherd, G.M. (2004). Modeldb: A database to support computational neuroscience. *Journal Computational Neuroscience*, 17(1), 7–11. doi:10.1023/B:JCNS.0000023869.22017.2e.
- Hocped, G., Legros, B., Van Bogaert, P., Grenez, F., Nonclercq, A. (2013). Early detection of epileptic seizures based on parameter identification of neural mass model. *Computer Biology Medicine*, 43(11), 1773–1782. doi:10.1016/j.compbiomed.2013.08.022.
- Holt, G. (1997). In *A critical reexamination of some assumptions and implications of cable theory in neurobiology*. PhD thesis: California Institute of Technology. URL <http://inc.usc.edu/holt/papers/thesis/>.
- Hutt, A. (2012). The population firing rate in the presence of GABAergic tonic inhibition in single neurons and application to general anaesthesia. *Cognitive neurodynamics*, 6(3), 227–37. doi:10.1007/s11571-011-9182-9.
- Hutt, A. (2013). The anesthetic propofol shifts the frequency of maximum spectral power in eeg during general anesthesia: analytical insights from a linear model. *Front Computational Neuroscience*, 7, 2. doi:10.3389/fncom.2013.00002.
- Izhikevich, E.M. (2007). In *Dynamical Systems in Neuroscience The Geometry of Excitability and Bursting*: Computational neuroscience, vol First. MIT Press. URL <http://www.amazon.com/dp/0262514206>.
- Jansen, B.H., & Rit, V.G. (1995). Electroencephalogram and visual evoked potential generation in a mathematical model of coupled cortical columns. *Biology Cybernetics*, 73(4), 357–366.
- Liley, D.T.J., Cadusch, P.J., Dafilis, M.P. (2002). A spatially continuous mean field theory of electrocortical activity. *Network (Bristol England)*, 13(1), 67–113.
- Manwani, A., & Koch, C. (1999). Detecting and estimating signals in noisy cable structure, i: neuronal noise sources. *Neural Computation*, 11(8), 1797–1829.
- Marreiros, A.C., Daunizeau, J., Kiebel, S.J., Friston, K.J. (2008). Population dynamics: variance and the sigmoid activation function. *NeuroImage*, 42(1), 147–57. doi:10.1016/j.neuroimage.2008.04.239.
- Meisler, M.H., & Kearney, J.A. (2005). Sodium channel mutations in epilepsy and other neurological disorders. *Journal Clinical Investigation*, 115(8), 2010–2017. doi:10.1172/JCI25466.
- Moran, R., Pinotsis, D.A., Friston, K. (2013). Neural masses and fields in dynamic causal modeling. *Front Computational Neuroscience*, 7, 57. doi:10.3389/fncom.2013.00057.
- Ostojic, S., & Brunel, N. (2011). From spiking neuron models to linear-nonlinear models. *PLoS computational biology*, 7(1)(e1001), 056. doi:10.1371/journal.pcbi.1001056.
- van Putten M.J., & Zandt B.J. (2013). Neural Mass modeling for predicting seizures. *Clinical Neurophysiology*. doi:10.1016/j.clinph.2013.11.013.
- Robinson, P.A., Rennie, C.J., Wright, J.J., Bahramali, H., Gordon, E., Rowe, D.L. (2001). Prediction of electroencephalographic spectra from neurophysiology. *Physics Review E Statistics Nonlinear Soft Matter Physics*, 63(2 Pt 1)(021), 903.
- Pa, R., Robinson, W., Wu, H., Kim, J.W. (2008). Neural rate equations for bursting dynamics derived from conductance-based equations. *Journal of theoretical biology*, 250(4), 663–72. doi:10.1016/j.jtbi.2007.10.020.
- Schevon, C.A., Ng, S.K., Cappell, J., Goodman, R.R., McKhann, G. J., Waziri, A., Branner, A., Sosunov, A., Schroeder, C.E., Emerson, R.G. (2008). Microphysiology of epileptiform activity in human neocortex. *Journal Clinical Neurophysiol*, 25(6), 321–330. doi:10.1097/WNP.0b013e31818e8010.
- Shriki, O., Hansel, D., Sompolinsky, H. (2003). Rate models for conductance-based cortical neuronal networks. *Neural computation*, 15(8), 1809–41. doi:10.1162/08997660360675053.
- Somjen, G. (2004). In *Ions in the Brain: Normal Function, Seizures and Stroke*. USA: Oxford University Press. <http://books.google.nl/books?id=yaNrAAAAMA AJ>.
- Somjen, G.G. (2001). Mechanisms of spreading depression and hypoxic spreading depression-like depolarization. *Physiology Reviews*, 81(3), 1065–1096.
- Stead, M., Bower, M., Brinkmann, B.H., Lee, K., Marsh, W.R., Meyer, F.B., Litt, B., Van Gompel, J., Worrell, G.A. (2010). Microseizures and the spatiotemporal scales of human partial epilepsy. *Brain*, 133(9), 2789–2797. doi:10.1093/brain/awq190.
- Tjepkema-Cloostermans, M.C., Hindriks, R., Hofmeijer, J., van Putten MJAM (2013). Generalized periodic discharges after acute cerebral ischemia: Reflection of selective synaptic failure?. *Clinical Neurophysiol*. doi:10.1016/j.clinph.2013.08.005.
- Touboul, J., Hermann, G., Faugeras, O. (2012). Noise-induced behaviors in neural mean field dynamics. *SIAM Journal on Applied Dynamical Systems*, 11(1), 49–81. doi:10.1137/110832392. <http://epubs.siam.org/doi/pdf/10.1137/110832392>.
- Victor, J.D., Drover, J.D., Conte, M.M., Schiff, N.D. (2011). Mean-field modeling of thalamocortical dynamics and a model-driven approach to EEG analysis. *Proceedings of the National Academy of Sciences of the United States of America* 108 Suppl, 15, 631–8. doi:10.1073/pnas.1012168108.
- Visser, S., & Van Gils, S. (2014). Lumping Izhikevich neurons. *EPJ Nonlinear Biomedical Physics*, 2(1), 6. doi:10.1140/epjnbp19. URL <http://www.epjnonlinearbiomedphys.com/content/2/1/6>.
- Wilson, H.R., & Cowan, J.D. (1972). Excitatory and inhibitory interactions in localized populations of model neurons. *Biophysical journal*, 12(1), 1–24. doi:10.1016/S0006-3495(72)86068-5.
- Zandt, B.J., ten Haken, B., van Dijk, J.G., van Putten, M. J.A.M. (2011). Neural dynamics during anoxia and the “wave of death”. *PLoS One*, 6(7)(e22), 127. doi:10.1371/journal.pone.0022127.
- Ziburkus, J., Cressman, J.R., Barreto, E., Schiff, S.J. (2006). Interneuron and pyramidal cell interplay during *in vitro* seizure-like events. *Journal Neurophysiology*, 95(6), 3948–3954. doi:10.1152/jn.01378.2005.